

Article

Airflow Velocity Designing for Air Classifier of Manufactured Sand Based on CPFD Method

Shuhua Peng¹, Yu Wu^{2,*}, Jing Tao³ and Jianbin Chen⁴

¹ School of Mechanics and Civil Engineering, China University of Mining and Technology, Xuzhou 221116, China; pengshuhua@cumt.edu.cn

² State Key Laboratory for Geomechanics and Deep Underground Engineering, China University of Mining and Technology, Xuzhou 221116, China

³ School of Mechanical Engineering, Sichuan University of Science and Engineering, Zigong 643000, China; taojing@suse.edu.cn

⁴ Guizhou Railway Construction Technology Development Co., Ltd., Guiyang 550081, China; scjb1981@126.com

* Correspondence: wuyu@cumt.edu.cn

Abstract: Airflow classification is the key technology for the dry separation of manufactured sand. To solve the problem of low separation accuracy and poor gradation grade, the classification process of manufactured sand under different inlet and outlet airflow velocities changes in the multi-air inlet classifier is simulated by using Barracuda based on Computational Particle Fluid Dynamics (CPFD) method. The influence of various airflow velocity in air inlets and outlet on the sand classification is analyzed. The optimal combination of airflow velocity that meets the design goals is obtained. The results show that the airflow velocity and location of the air inlet and outlet have a significant impact on medium-grained (0.15~1.18 mm) and fine-grained (0.075~0.3 mm) sand. Adjusting the airflow velocity at air inlet 2 and air outlet can most effectively change the overall sand separation effect, while 41 m/s (inlet 2) and 6 m/s (outlet) would be the best velocity combination.

Keywords: air classifier; airflow velocity; CPFD; gas–particle flow; separator



Citation: Peng, S.; Wu, Y.; Tao, J.; Chen, J. Airflow Velocity Designing for Air Classifier of Manufactured Sand Based on CPFD Method. *Minerals* **2022**, *12*, 90. <https://doi.org/10.3390/min12010090>

Academic Editors: Chiharu Tokoro, Shigeshi Fuchida, Yutaro Takaya and Saeed Farrokhpay

Received: 5 November 2021

Accepted: 11 January 2022

Published: 13 January 2022

Publisher's Note: MDPI stays neutral with regard to jurisdictional claims in published maps and institutional affiliations.



Copyright: © 2022 by the authors. Licensee MDPI, Basel, Switzerland. This article is an open access article distributed under the terms and conditions of the Creative Commons Attribution (CC BY) license (<https://creativecommons.org/licenses/by/4.0/>).

1. Introduction

As a short-term non-renewable construction aggregate, natural sand has been nearly exhausted after decades of high-intensity mining. Meanwhile, governments around the world have issued a series of restrictions on mining natural sand for flood control, shipping safety, and environmental protection considerations, resulting in even more scarce natural sand resources available for exploitation [1–3]. Therefore, it is necessary to promote the use of manufactured sand as a substitute vigorously [4–6]. In the manufactured sand production process, classification is an essential basic operation. It separates the crushed sand into multiple components with different particle size distributions. Both wet and dry state classification are widely used in industry. Compared with the wet process, the dry process is less affected by water source, climate, and temperature, and can save water resources [5]. Moreover, it can also install stone powder recovery equipment at the air flow outlet to help decrease pollution. The secondary recycled stone powder can also be used to improve the performance of concrete [7,8]. Under the current situation of advocating environmental protection and increasing demand for the grading quality of manufactured sand, dry air classification is increasingly favored by the industry. The gravity air classifier is a core equipment of the manufactured sand making process, and its classification ability will directly affect the quality and output of the aggregate.

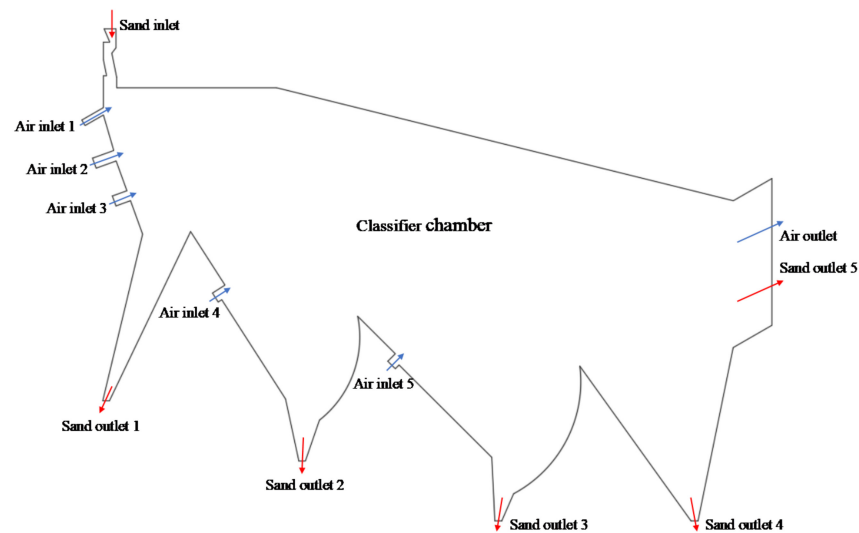
In the manufactured sand industry, the research and development of gravity air classifiers have begun to take shape, but it is still in the rough stage. Most of them are only used to screen stone powder, or divide sand into three grades: coarse sand, fine sand, and stone

powder. The gradation of the finished manufactured sand is poor, and the separation effect of the equipment needs to be improved. Based on simulation methods and software such as CFD and CPFD, scholars have made some progress in the field of gas–solid two-phase flow simulation of air classifiers. The airflow field, particle trajectory, and various factors affecting the separation effect are studied. Qianpu Wang et al. [9] simulated the particle classification process in a cross-flow air classifier with the help of FLUENT and found that vortex, particle collision, turbulence, and inlet velocity are the main factors affecting separation efficiency. Kolacz, J [10] studied the airflow field in the air classifier with FLUENT and pointed out the weaknesses limiting its classification performance, which can be used to optimize the structural parameters of the classifier in the future. Yanyan Li et al. [11] used FLUENT to study the influence of gravity air classifier structure, air velocity and feed rate on classification efficiency, and finally obtained the optimal dispersion structure. H. A. Petit [12] used CFD-DEM to simulate the classification process of manufactured sand in the cross-flow air classifier and evaluated the applicability of dust separation. Horacio A. Petit et al. [13] used CFD-DPM to design and simulate the internal classification mechanism of the inclined plane air classifier. The flow field characteristics and particle trajectories are studied, and the structure is optimized to improve the particle size distribution of manufactured sand. By assuming and adjusting the numerical model's initial conditions and structural parameters, combined with a series of physical control experiments, the feasibility of numerical simulation for predicting the airflow classification process of particles is verified [14–19]. Scholars also pointed out the shortcomings of the gravity air classifier [20,21]. However, these studies mainly focus on airflow classification in fields such as grains and garbage, and there are few studies on manufactured sand [22–29]. Meanwhile, research on multi-air inlet equipment is still lacking in the field of air classification of manufactured sand, and previous studies have mainly focused on the single air inlet structure.

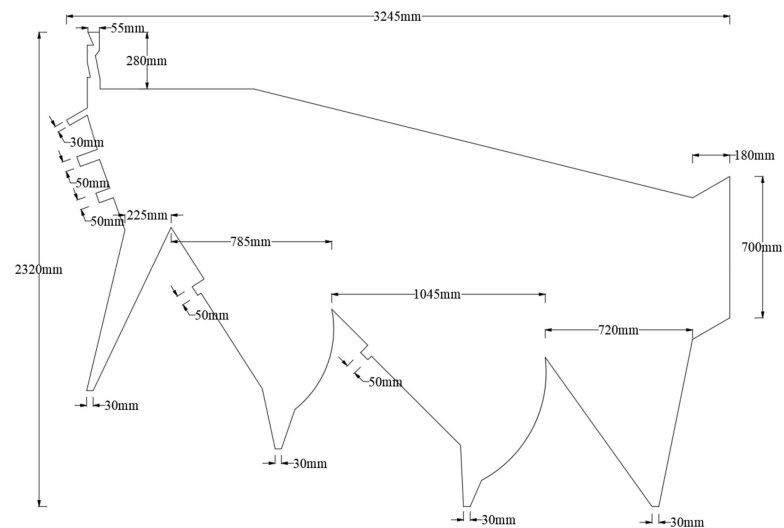
Therefore, focusing on the effect of the airflow velocity change of multi air inlet equipment on the sand separation rate, with the help of Barracuda VR (Virtual Reactor), the air classification process of manufactured sand was simulated. Under the change of airflow velocity of different air inlets and outlet, the movement state of varying particle size sand and the changing trend of separation rate of each sand outlet were investigated. Finally, the optimal airflow velocity combination that meets the design goal was obtained. This study will provide guidance for the airflow velocity design of the manufactured sand air classifier.

2. Geometric Model

The geometric model of the air classifier simulated in this paper is shown in Figure 1a,b, respectively, and shows the structural composition and size of the geometric model. The model was designed and made by Guizhou Railway Construction Technology Development Co., Ltd., Guiyang, China. The equipment is a multi-air inlet structure, 3.245 m long, 2.320 m high, with a thickness of 1 m. The model structure remains unchanged in the thickness direction. It contains one sand inlet, five air inlets, one air outlet, and four sand outlets. The sand inlet is 55 mm wide, the air inlet 1 is 30 mm wide, the remaining air inlets are both 50 mm wide, the air outlet width is 700 mm, and the sand outlets are all 50 mm wide. The inclined sidewall at the air inlets 1, 2, and 3 can fit the particle trajectory of sand so that the airflow can more effectively affect the sand movement. The airflow at air inlets 4 and 5 can effectively prolong the movement time of 0–1.18 mm sand, increase its lateral displacement and make its classification more sufficient. Sand with different particle sizes can be separated into the specified sand outlet by adjusting the air velocity at the air outlet and five air inlets.



(a) The structural composition of the geometric model



(b) The structure size of the geometric model

Figure 1. Geometric model of air classifier.

Table 1 and Figure 2 show the particle size distribution of the fed manufactured sand. In the table, in accordance with construction engineering norms, the sand is divided into seven particle sizes according to the diameter. The particle size distribution of manufactured sand is continuous and wide, which limits its classification accuracy. This equipment cannot accurately separate the sand of each particle size grade by classifying it only once. It performs cross-particle size classification, as shown in Figure 3. Each outlet collects sand of two or three particle size ranges. After that, simple secondary separation can be used to accurately separate the sand discharged from each outlet. The standard of the target separation particle size and the separation rate of each sand outlet are shown in Table 2. The separation rate is obtained by dividing the cumulative mass of the target particle size at the sand outlet by the gross mass. Since the sand outlet 4 is farthest from the sand inlet and air inlets, it is difficult to control the particle size composition of the collected sand. In addition, the amount of sand collected here is small, so the target separation rate of outlet 4 is not strictly required.

Table 1. The particle size distribution of the fed manufactured sand.

Diameter (mm)	Cumulative (%)
0.075	5.2
0.15	8.6
0.3	15.2
0.6	29.9
1.18	53
2.36	82.8
4.75	100

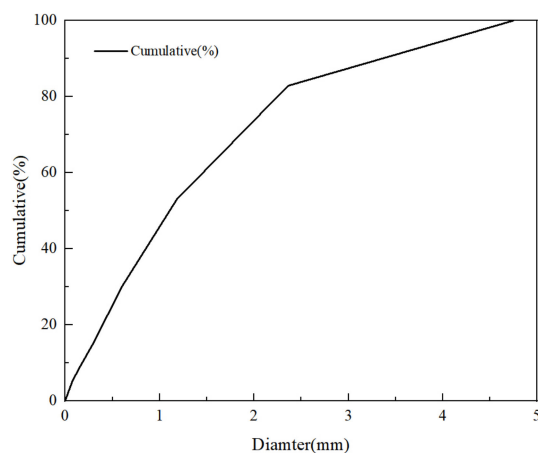


Figure 2. Particle size distribution.

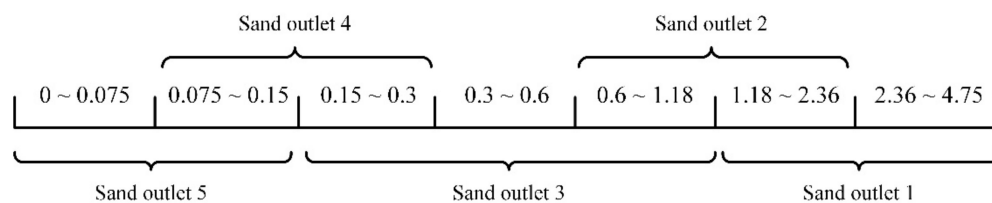


Figure 3. Target particle size of each outlet.

Table 2. Target particle size of each outlet.

Sand Outlet	1	2	3	4	5
Sand class	Coarse grain	Medium-coarse grain	Medium grain	Fine grain	Powder grain
Target particle size (mm)	1.18~4.75	0.6~2.36	0.15~1.18	0.075~0.3	0~0.15
Target separation rate (%)	90	90	90	75	90

The air classifier’s working principle is that sand particles of different particle sizes have varied trajectories and settling velocities as a result of gravity and air flow. In this multi-air inlet structure, the manufactured sand is fed from the sand inlet, and the lighter powder and fine sand in the particle stream are blown backward and separated with the help of the airflow from air inlets 1 and 2. The airflow at the air inlet 3 affects the separation effect of medium-coarse and medium sand, and further strengthens the lateral movement of powder and fine particles. Air inlets 4 and 5 are arranged at the left partition of sand outlets 2 and 3 to assist in subdividing medium and fine sand in subsequent grading so that they can fall into the corresponding sand outlet. In addition, the air is drawn from the air outlet to improve the flow field and recover stone powder.

3. Numerical Methods

3.1. Governing Equations for CFPD

Manufactured sand containing a large number of particles quickly and in full-size distribution. In the CFPD method, for the gas–solid two-phase flow [30]:

$$\varepsilon_p + \varepsilon_g = 1 \quad (1)$$

where ε_p is the volume fraction of the particle phase, ε_g is the volume fraction of the gas phase. The gas continuity equation is:

$$\frac{\partial(\varepsilon_p \rho_g)}{\partial t} + \nabla(\varepsilon_p \rho_g \vec{u}_g) = 0 \quad (2)$$

where ρ_g is the gas density, \vec{u}_g is the gas velocity. The gas phase momentum equation is:

$$\frac{\partial(\varepsilon_p \rho_g \vec{u}_g)}{\partial t} + \nabla(\varepsilon_p \rho_g \vec{u}_g \vec{u}_g) = -\nabla p - \vec{F} + \varepsilon_p \rho_g \vec{g} + \nabla \varepsilon_p \tau_g \quad (3)$$

where p is the gas pressure, τ_g is the stress tensor, \vec{g} is acceleration of gravity, \vec{F} is momentum exchange rate of gas–solid phase per unit volume. The particle phase momentum equation is:

$$\frac{d\vec{u}_p}{dt} + D_p(\vec{u}_g - \vec{u}_p) - \frac{1}{\rho_p} \nabla p + \vec{g} - \frac{1}{\varepsilon_p \rho_g} \nabla \tau_p \quad (4)$$

where \vec{u}_p is the particle velocity, ρ_p is the particle density.

3.2. Numerical Simulation Model

We imported the CAD model of the equipment into Pro Engineer, built the 3D model, and then imported it into Barracuda for meshing and simulation. Since the model structure remains unchanged in the thickness direction, the thickness does not affect the simulation. To reduce the computing time, the thickness is set to 200 mm, and the feed mass flow rate of sand is also reduced to one fifth.

Figure 4 shows the simulation model, the sand inlet, air inlet, and air outlet are red, and the sand outlet is yellow, the whole domain was divided into 37,878 cells. As shown in Figure 5, the simulation model was chosen after the mesh independence test. Models with grid numbers of 37,878, 77,252, and 155,430 are used to simulate the air flow classification process, according to the conditions in Tables 3 and 4. We can see that the cumulative mass and separation rate between the model of 37,878 cells and other models are very similar. Reducing the number of grids can greatly reduce the simulation time, so 37,878 grids were chosen to simulate the air flow classification process of manufactured sand in this paper.

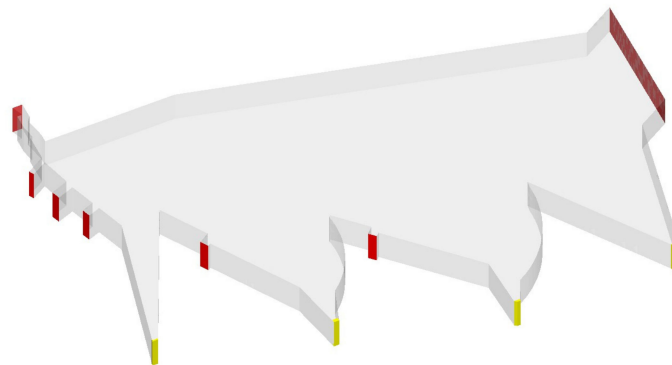


Figure 4. Simulation model of the air classifier.

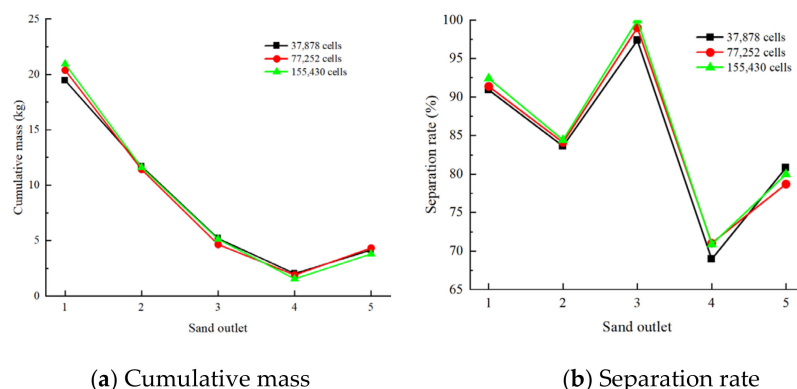


Figure 5. Cumulative mass and separation rate under different grid numbers.

Table 3. Parameter settings.

Parameter	Value
Gas density	1.225 kg/m ³
Gas dynamic viscosity	1.79 × 10 ⁻⁵ kg/(m·s)
Sand density	2640 kg/m ³
Sand diameter	0~4.75 mm
Sand feed mass flow rate	7.35 kg/s
Sand feed rate	1 m/s
Drag model	Wen-Yu
Close pack volume fraction	0.6
Maximum momentum redirection from collision	40%
Normal-to-wall momentum retention	0.5
Tangent-to-wall momentum retention	0.85
Time step	0.002 s

Table 4. The airflow velocity of the original scheme.

Airflow	Air Inlet					Air Outlet (V ₆)
	1 (V ₁)	2 (V ₂)	3 (V ₃)	4 (V ₄)	5 (V ₅)	
Airflow velocity (m/s)	35	35	32	34	20	8

3.3. Boundary Condition

In simulation parameter settings, the fluid flow was set to isothermal and incompressible, and the temperature was fixed at 300 K. The manufactured sand particles are assumed to be spherical and evenly distributed in the sand inlet plane during feeding. Chemical reaction is not taken into account in the setting because only particle classification is done.

Set the air as the gas phase and the manufactured sand as the solid phase. The air inlets, sand inlet, sand outlets, and air outlet are connected with the atmosphere. The air inlets are set as the velocity inlet, and only the gas phase is allowed to pass. The sand inlet, sand outlets, and air outlet allow the gas and solid phases to pass through, the sand inlet is set as the velocity inlet, and the air outlet is set as the velocity outlet. The processing capacity of the equipment is designed to be 36.75 kg/s, however after lowering the thickness of the model during simulation, it is decreased to 7.35 kg/s. The pressure boundary condition of the equipment is the standard atmospheric pressure (101,325 Pa). Use Barracuda VR to simulate the 7-s air classification process of manufactured sand in the equipment. A large eddy simulation (LES) was used, in which large eddies were directly calculated. The subgrid-scale (SGS) turbulence was calculated using the Smagorinsky method [31]. Table 3 shows the relevant parameter settings of the simulation software.

3.4. Simulation Results of the Original Scheme

Table 4 is the original scheme, which is a preliminary determination of the airflow velocity combination used for manufactured sand classification after several simulations. Where $V_1 \sim V_5$ are the airflow velocity of the sand outlet corresponding to the number, and V_6 is the airflow velocity of the air outlet. Since the air inlet 5 is located on the upper side of the sand outlet 3, it can only affect the distribution of 0–0.6 mm sand and a minor portion of 0.6–1.18 mm sand. The mass of it accounts for less than 50% of the total sand, so the velocity here is set to be small. The simulation results of the airflow velocity scheme are obtained and processed. Figure 6 is a distribution map of sand in each particle size range during the classification process, in which the red part represents the particles within the particle size range. Each sand outlet collects two or three particle size ranges, as shown in Figure 3. In Figure 6, the sand sorted by outlet 1 is (f) and (g), outlet 2 is (e) and (f), outlet 3 is (d) and a small amount of (c) and (e), outlet 4 corresponds to (b) and (c), outlet 5 is the particle size shown in (a) and (b).

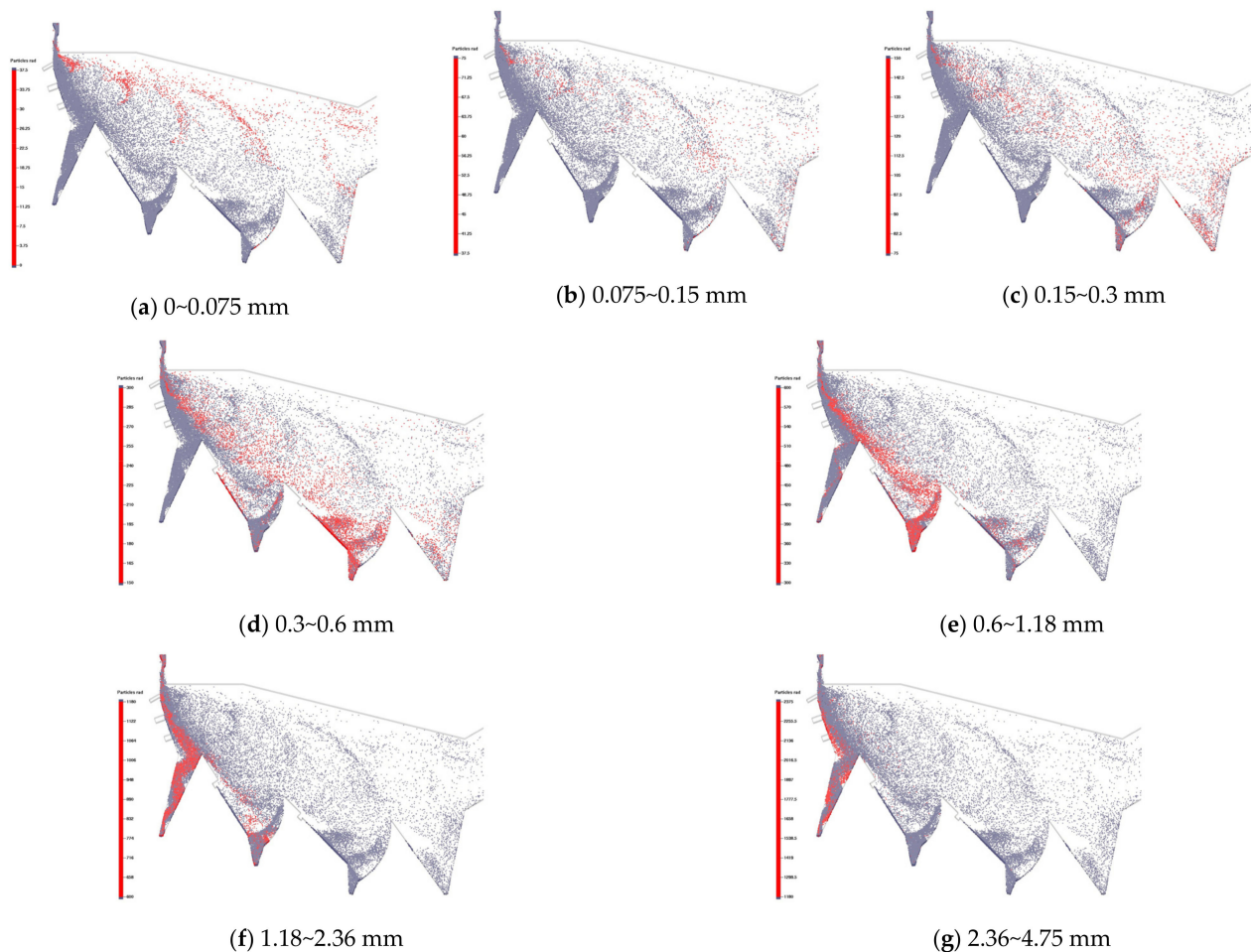


Figure 6. Sand distribution of various particle sizes under the original scheme.

Figure 7 shows the cumulative mass of sand at each sand outlet. We can find that the sand is mainly concentrated in outlets 1 and 2. This is because the mass of coarse and medium-coarse sand collected at the two outlets accounts for a large proportion. The remaining sand is collected at outlets 3~5, of which the sand at outlet 4 is the least. Figure 8 shows the simulation results of each sand outlet's separation rate of the target particle size under the original scheme. According to the sand distribution, the classification ability of the multi-air inlet structure is improved compared with the traditional single air inlet structure, and the sand can be subdivided according to the particle size grade. The air

inlets at different positions can affect the whole classification process of sand. Comparing the sand distribution and separation rate, we can see that the separation effect of sand outlets 1 and 3 is better and meets the design requirements. In contrast, the separation rate of the remaining sand outlets does not reach the target. We can find the reason from Figure 6 that the 0.3~0.6 mm particles are too dispersed during the separation process and are distributed in outlets 2~4. Although outlet 3 has the highest separation rate, it has a poor separation impact for sand with a diameter of 0.3~0.6 mm. Some 0.3~0.6 mm sand is blown to outlet 4, so outlet 4 has the poorest separation rate. Meanwhile, particles with a particle size of 0.15~0.3 mm are blown to outlet 5 due to excessive airflow velocity, reducing the separation rate.

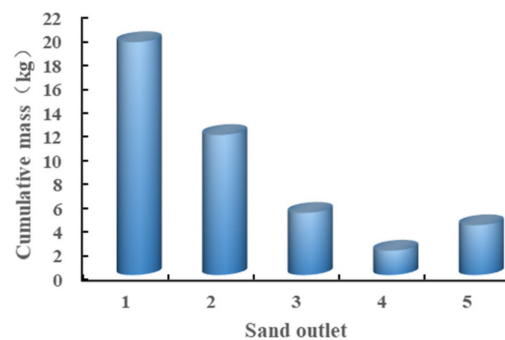


Figure 7. Cumulative mass of sand under the original scheme.

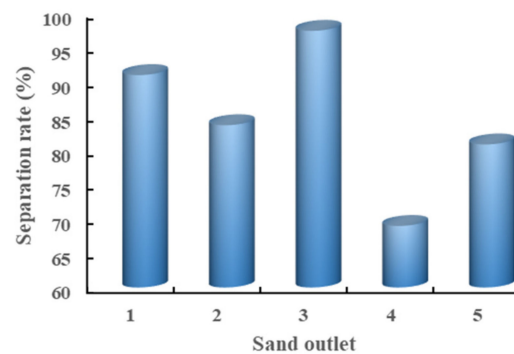


Figure 8. Sand separation rate of target particle size under the original scheme.

4. The Effects of Airflow Velocity on the Sand Classification

4.1. Simulation Scheme

The design goal of the equipment is to classify the manufactured sand according to the particle size. From the results of the original plan, the overall classification effect of the equipment did not meet the overall target separation rate, and the airflow velocity of each air inlet and outlet still needs subsequent adjustment. Therefore, the following will study the effects of airflow velocity changes at different air inlets on the separation rate. The simulation scheme is shown in Table 5, including 30 sets of simulations.

Table 5. Simulation schemes of different airflow velocity combinations.

Airflow	Air Inlet					Air Outlet (V ₆)
	1 (V ₁)	2 (V ₂)	3 (V ₃)	4 (V ₄)	5 (V ₅)	
Airflow velocity (m/s)	24/29.5/35/ 40.5/46	35	32	34	20	8
	35	24/29.5/35/ 40.5/46	32	34	20	8
	35	35	22/27/32/ 37/42	34	20	8
	35	35	32	23/28.5/34/ 39.5/45	20	8
	35	35	32	34	14/17/20/ 23/26	8
	35	35	32	34	20	5/6.5/8/ 9.5/11

4.2. Results and Discussion

Figure 9 shows the changing trend in the separation rate of manufactured sand at each sand outlet when the airflow velocity at the air inlets 1, 2, and 3 changes. By comparison, it is found that the change in the airflow velocity at air inlet 2 has the most significant impact on the overall airflow classification effect. The increase in the airflow velocity of each air inlet and outlet will improve the separation rate of sand outlets 1 and 2, and inlet 2 has the most obvious effect. When V₂ increases from 24 m/s to 46 m/s, the separation rates of outlets 1 and 2 rise from 75.35% and 55.39% to 99.75% and 91.53%, respectively. The reason is that the medium-grain (0.15~1.18 mm) sand content in outlets 1 and 2 is reduced. Meanwhile, we can see that the change in airflow velocity at the air inlets 1, 2, and 3 has little effect on the sand separation at outlets 3 and 5, but the impact on outlet 4 is significant. For example, the increase in V₁ and V₂ caused the sand outlet 4 separation rate to fall from 77.85% and 81.41% to 56.55% and 48.38%, respectively. Since the cumulative mass of sand in outlet 4 is tiny, a change in particle size distribution can easily impact its separation rate.

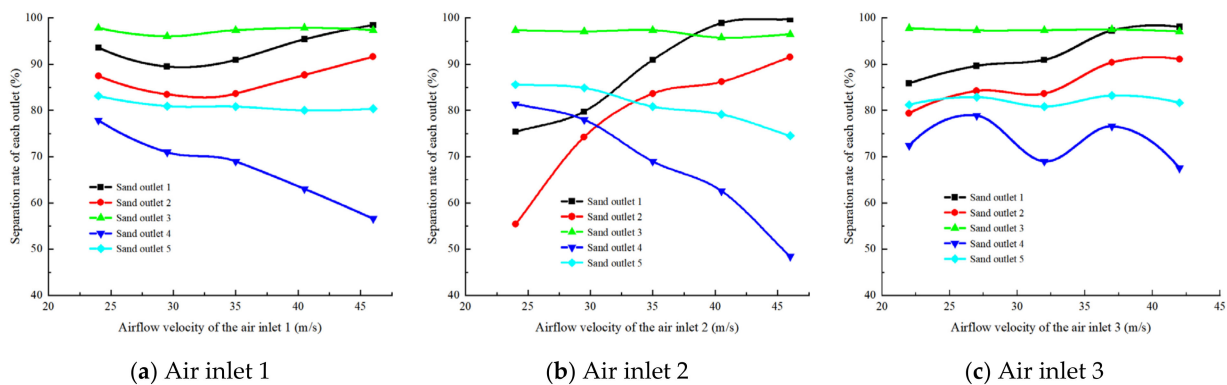


Figure 9. The change curve of the separation rate of each outlet under the change of the airflow velocity of the air inlets 1~3.

Figure 10 is a comparison diagram of the variation curves of the separation rate of each outlet when the airflow velocity of air inlets 4 and 5 changes. It can be seen from Figure 10 that the change in the airflow velocity has little effect on the overall separation effect. At the same time, by comparing the separation rate of sand outlet 4, we can see that the changes of V₃, V₄, and V₅ will cause the separation rate of the outlet to show an unstable wave-shaped change trend.

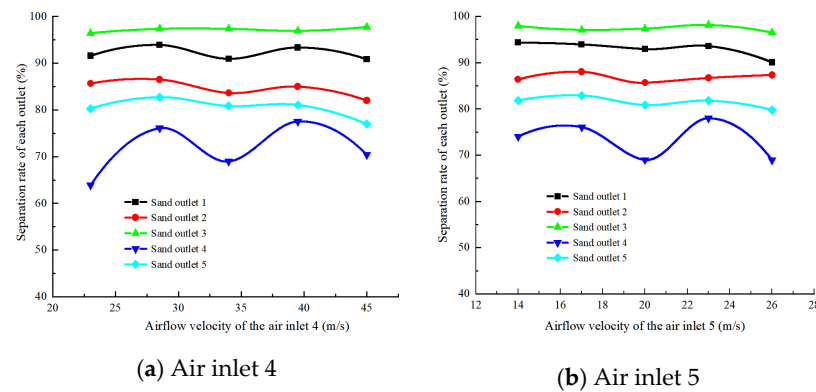


Figure 10. Variation curve of sand separation rate under the change of airflow velocity at air inlets 4 and 5.

Figure 11 shows the variation curves of the separation rate of each outlet under the change in the airflow velocity of the air outlet. We can see that changing the velocity of the outlet airflow has a big impact on the separation rate of each sand outlet. The separation rate of sand outlets 1, 2, and 3 will increase synchronously with the airflow velocity. When the airflow velocity increases to 11 m/s, the separation rate of outlets 1 and 2 increases to more than 92%, and the separation rate of outlet 3 even reaches 99.82%. On the contrary, the separation rate of sand outlets 4 and 5 decreases significantly with increased airflow velocity. When $V_6 = 11$ m/s, the separation rate reaches its lowest, and the downward trend is also the most obvious. Figure 12 shows each particle size’s cumulative mass change diagram at sand outlets 4 and 5. We can find that when the airflow velocity at the wind outlet increases, a large amount of fine-grained (0.075~0.3 mm) sand is blown from sand outlets 4 to 5, resulting in a significant reduction in the separation rate.

Furthermore, despite the fact that the change in air velocity at each tuyere appears to have minimal influence on the separation rate of outlet 3, the mass proportion of sand in the internal particle size ranges of 0.15~0.3, 0.3~0.6, and 0.6~1.18 mm has changed. For example, Table 6 shows the change in sand particle size distribution at outlet 3 as the velocity of air inlet 1 changes, with the increase of air velocity, the mass proportion of 0.6~1.18 mm sand grows significantly, while the mass proportion of 0.15~0.3 mm and 0.3~0.6 mm sand drops.

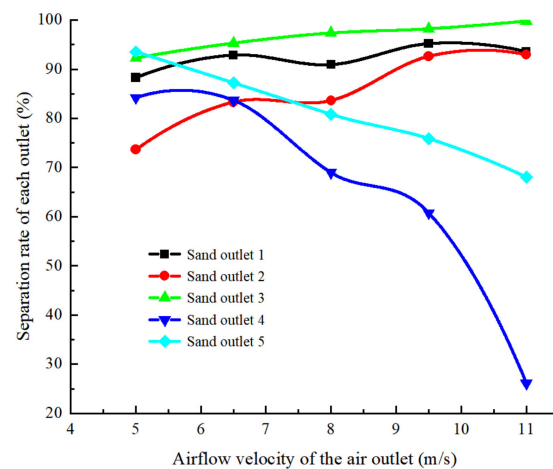


Figure 11. Variation curve of sand separation rate under the change of air outlet velocity.

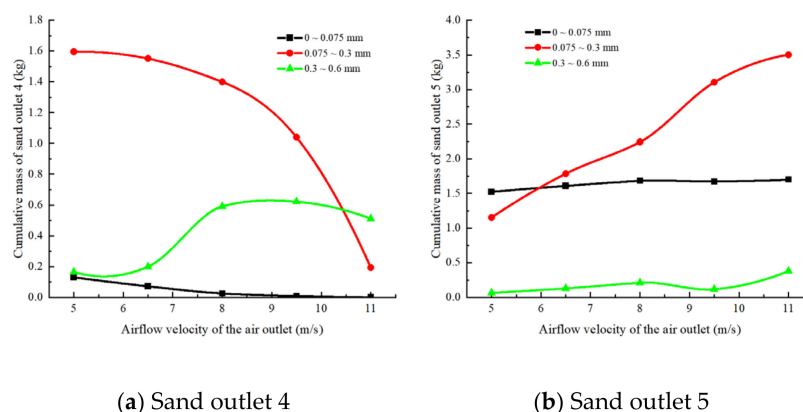


Figure 12. Cumulative mass variation curve of each particle size of sand outlets 4 and 5.

Table 6. Sand particle size distribution at outlet 3 under the change of air velocity at air inlet 1.

Velocity (m/s)	Mass Proportion of Each Particle Size (%)			Separation Rate (%)
	0.15~0.3 mm	0.3~0.6 mm	0.6~1.18 mm	
24	19.91	64.52	13.4	97.84
29.5	23.4	62.09	10.55	96.05
35	22.49	62.91	11.96	97.37
40.5	19.31	59.61	18.93	97.86
46	15.34	54.13	27.88	97.36

Comparing the influence of the air velocity change of each air inlet and outlet on the sand separation rate, it can be found that the air velocity change of air inlet 2 and outlet has a greater impact on the overall classification effect. The velocity of air inlet 2 has a more significant effect on medium-grained (0.15~1.18 mm) and fine-grained (0.075~0.3 mm) sand. The air outlet velocity significantly influences the airflow classification of fine particles (0.075~0.3 mm).

5. Simulation of the Optimal Air Velocity Combination

5.1. Simulation Scheme

From the above research on the effect of the velocity change of the air inlets and outlet on the sand classification, the law of the sand separation rate was obtained. According to it, the simulation scheme shown in Table 7 was designed, which included 12 sets of simulations. It only changed the velocity at the air outlet and inlet 2, and left others that have little impact on sand classification unchanged.

Table 7. Airflow velocity adjustment simulation scheme.

Case	V ₁ (m/s)	V ₂ (m/s)	V ₃ (m/s)	V ₄ (m/s)	V ₅ (m/s)	V ₆ (m/s)
1	35	37	32	34	20	6/7/9/10
2	35	39	32	34	20	6/7/9/10
3	35	41	32	34	20	6/7/9/10

5.2. Results and Discussion

Table 8 shows the simulation results for the separation rate of manufactured sand for different airflow velocity combinations. By comparison, we can find that when V₂ = 41 m/s and V₆ = 6 m/s, there is an optimal airflow velocity combination scheme.

Table 8. Simulation results of separation rate of different airflow velocity combinations.

V_2 (m/s)	V_6 (m/s)	Separation Rate (%)				
		Sand Outlet 1	Sand Outlet 2	Sand Outlet 3	Sand Outlet 4	Sand Outlet 5
37	6	92.9	81.3	94.5	77.6	89.5
	7	93.7	84.3	95.8	73.4	84.6
	9	95.1	91.4	98.6	58.3	75.2
	10	95.9	94.4	99.5	48.0	70.9
39	6	96.0	85.0	93.2	76.0	87.8
	7	96.7	87.8	96.8	71.6	83.8
	9	98.0	93.5	98.4	55.0	74.4
	10	98.1	95.6	99.4	43.6	68.8
41	6	98.1	90.2	95.0	75.1	89.0
	7	98.1	91.7	95.7	67.9	82.3
	9	98.9	93.7	98.1	49.5	73.3
	10	99.1	95.4	99.2	40.8	66.8

Figure 13 is the distribution diagram of each particle size range of sand during the air classification process of the optimal scheme, and Figures 14 and 15, respectively, show the comparison of the cumulative mass and separation rate of each sand outlet between the original scheme and the optimized scheme. We can find that the overall distribution of sand is more appropriate, and the classification effect is substantially improved, as compared to the original scheme. The cumulative mass and separation rate of sand outlet 1 and sand outlet 2 have changed significantly, which is caused by the reduction of the mass of sand with particle size of 0.6–1.18 mm in sand outlet 1. The cumulative mass change of sand at outlets 3, 4, and 5 is small, but the particle size composition of the sand here has a large change. It can be seen from the sand distribution map that the 0.3–0.6 mm particle distribution in the optimized scheme is relatively concentrated, which is mainly classified into outlet 3. The reduction in the separation rate of outlet 3 is due to the decrease in the airflow velocity at the air outlet, which causes a small number of powder particles (0–0.15 mm) to fall to outlet 3 instead of crossing the baffle. At the same time, due to the decrease in air flow velocity at the sand outlet, 0.15–0.3 mm particles are less blown to outlet 5. More sand with this particle size is collected by sand outlet 4, which leads to an improvement in the separation rate of sand outlet 4 and sand outlet 5. Therefore, all sand outlets of the equipment meet the design requirement with this combination of airflow velocity, and the manufactured sand can be precisely classified according to its particle size.

This paper only studies the airflow classification process of manufactured sand with a specific particle size distribution. However, we can use this strategy to develop a database that adjusts airflow velocity for different particle size distributions in practical projects. Furthermore, real-time monitoring of the particle size distribution of the sand at the inlet is carried out, and the airflow velocity is adjusted synchronously according to the database and monitoring results. This way, it can ensure that the air classifier can achieve the best classification effect in the actual engineering conditions where the particle size distribution of the feed sand is uncertain.

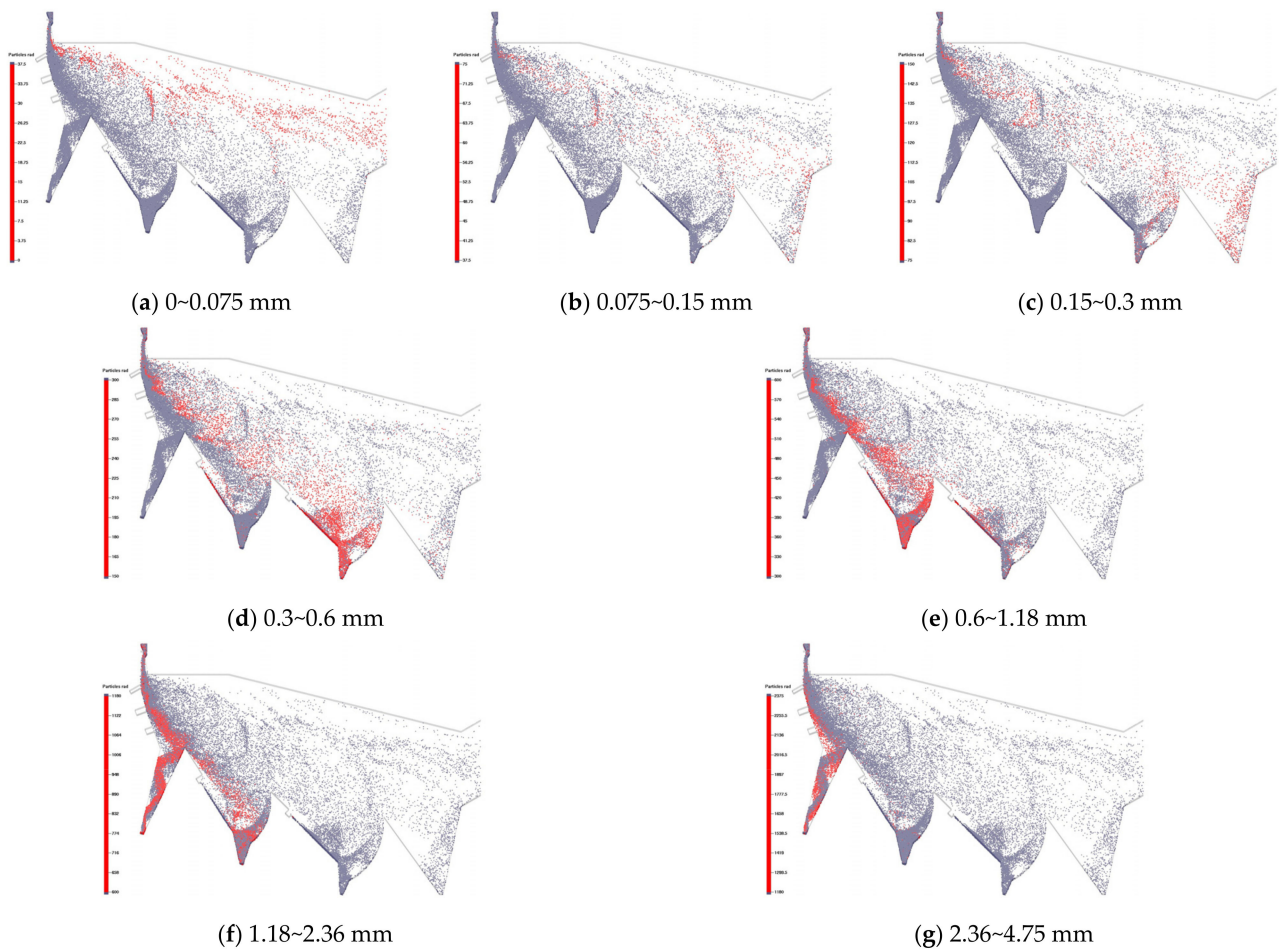


Figure 13. Sand distribution in the airflow classification process under the optimal scheme.

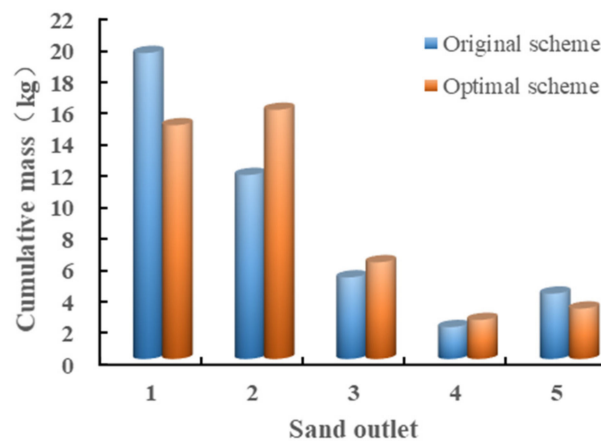


Figure 14. Comparison of the sand cumulative mass between the original and optimal scheme.

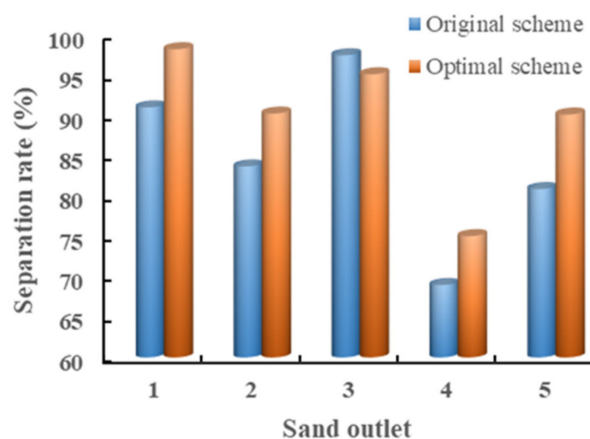


Figure 15. Comparison of the separation rate between the original and optimal scheme.

6. Conclusions

In this paper, the airflow classification process of manufactured sand in a multi-inlet air classifier is simulated under various airflow velocity combinations. The effect of changing air velocity on sand movement and separation rate is investigated, and the ideal air velocity combination that meets the design requirements is identified. The results allow the following conclusions to be drawn.

1. The multi-air inlet equipment can classify the manufactured sand finely according to its particle size grade. The original scheme can classify powder grain (0~0.15 mm) and coarse grain (1.18~4.75 mm), but the classification accuracy of medium grain (0.15~1.18 mm) needs to be improved.
2. Adjusting the airflow velocity of the air inlet 2 and the air outlet can most effectively change the classification effect. As the airflow velocity increases, the separation rate of sand outlets 1 and 2 increases, while outlet 4 is significantly reduced. An increase in the airflow velocity at the air outlet will significantly reduce the separation effect of the sand outlet 5. The interior particle size distribution changes with the air flow velocity, despite the fact that the separation rate at the outlet 3 changes little.
3. When $V_2 = 41$ m/s and $V_6 = 6$ m/s, there is an optimal airflow classification scheme that meets the design requirements under the condition of only changing the airflow velocity at the air inlet 2 and air outlet.
4. The impact of tuyere position and air velocity on different sand particle sizes is variable. Therefore, to achieve the best classification effect, we can monitor the particle size distribution of the inlet sand and adjust the airflow velocity in real-time according to it. The simulation research in this paper can guide the adjustment of airflow velocity in engineering problems.

Author Contributions: S.P. was responsible for data collection, analysis, and interpretation. Y.W. helped perform the analysis and guide the writing of the paper with constructive discussions. J.T. helped complete the numerical simulation. J.C. designed and provided the geometric model of the air classifier. S.P. wrote the first draft of the article. All authors have read and agreed to the published version of the manuscript.

Funding: This research received no external funding.

Data Availability Statement: The data used to support the findings of this study are available from the corresponding author upon request.

Acknowledgments: We acknowledge the supports from Guizhou Railway Construction Technology Development Co., Ltd. Guiyang, China.

Conflicts of Interest: The authors declare that they have no competing interests.

References

1. Gavriletea, M. Environmental Impacts of Sand Exploitation. Analysis of Sand Market. *Sustainability* **2017**, *9*, 1118.
2. Zhai, W.; Ding, J.; An, X.; Wang, Z. An optimization model of sand and gravel mining quantity considering healthy ecosystem in Yangtze River, China. *J. Clean. Prod.* **2020**, *242*, 118385. [[CrossRef](#)]
3. Leal Filho, W.; Hunt, J.; Lingos, A.; Platje, J.; Vieira, L.; Will, M.; Gavriletea, M. The Unsustainable Use of Sand: Reporting on a Global Problem. *Sustainability* **2021**, *13*, 3356. [[CrossRef](#)]
4. Zhang, M.; Wu, F.; Du, L.; Zhu, Q. Study on cleaner production technology and methods of high quality mechanism sand. *Inorg. Chem. Ind.* **2017**, *49*, 73–76.
5. Gonçalves, J.P.; Tavares, L.M.; Toledo Filho, R.D.; Fairbairn, E.M.R.; Cunha, E.R. Comparison of natural and manufactured fine aggregates in cement mortars. *Cem. Concr. Res.* **2007**, *37*, 924–932. [[CrossRef](#)]
6. Cortes, D.D.; Kim, H.K.; Palomino, A.M.; Santamarina, J.C. Rheological and mechanical properties of mortars prepared with natural and manufactured sands. *Cem. Concr. Res.* **2008**, *38*, 1142–1147. [[CrossRef](#)]
7. Cepuritis, R.; Jacobsen, S.; Onnela, T. Sand production with VSI crushing and air classification: Optimising fines grading for concrete production with micro-proportioning. *Miner. Eng.* **2015**, *78*, 1–14. [[CrossRef](#)]
8. Cepuritis, R.; Wigum, B.J.; Garboczi, E.J.; Mørtzell, E.; Jacobsen, S. Filler from crushed aggregate for concrete: Pore structure, specific surface, particle shape and size distribution. *Cem. Concr. Comp.* **2014**, *54*, 2–16. [[CrossRef](#)]
9. Wang, Q.; Melaaen, M.C.; De Silva, S.R. Investigation and simulation of a cross-flow air classifier. *Powder Technol.* **2001**, *120*, 273–280. [[CrossRef](#)]
10. Kolacz, J. Investigating flow conditions in dynamic air classification. *Miner. Eng.* **2002**, *15*, 131–138. [[CrossRef](#)]
11. Li, Y.; Zhang, X.; Shen, X.; Li, H.; Gao, K. Experiment and simulation study on optimized structure of a gravitational air classifier. *Int. J. Miner. Process.* **2015**, *141*, 44–50. [[CrossRef](#)]
12. Petit, H.A.; Irassar, E.F.; Barbosa, M.R. Evaluation of the performance of the cross-flow air classifier in manufactured sand processing via CFD–DEM simulations. *Comput. Part. Mech.* **2018**, *5*, 87–102. [[CrossRef](#)]
13. Petit, H.A.; Paulo, C.I.; Cabrera, O.A.; Irassar, E.F. Modelling and optimization of an inclined plane classifier using CFD–DPM and the Taguchi method. *Appl. Math. Model.* **2020**, *77*, 617–634. [[CrossRef](#)]
14. Lai, W.; Lu, W.; Chou, M. Sorting of fine powder by gravitational classification chambers. *Adv. Powder Technol. Int. J. Soc. Powder Technol.* **2009**, *20*, 177–184. [[CrossRef](#)]
15. Ueka, Y.; Matsui, M.; Inoue, E.; Mitsuoka, M.; Okayasu, T. Shape model of grain and straw using coupling elements and flight simulation of threshing unit of combine by discrete element method. *Eng. Agric. Environ. Food* **2014**, *7*, 34–39. [[CrossRef](#)]
16. Petit, A.; Cordoba, G.; Paulo, C.I.; Irassar, E.F. Novel air classification process to sustainable production of manufactured sands for aggregate industry. *J. Clean. Prod.* **2018**, *198*, 112–120. [[CrossRef](#)]
17. Jayarathna, C.K.; Balfe, M.; Moldestad, B.M.E.; Tokheim, L. Improved multi-stage cross-flow fluidized bed classifier. *Powder Technol.* **2018**, *342*, 621–629. [[CrossRef](#)]
18. Betz, M.; Gleiss, M.; Nirschl, H. Effects of Flow Baffles on Flow Profile, Pressure Drop and Classification Performance in Classifiers. *Processes* **2021**, *9*, 1213. [[CrossRef](#)]
19. Johansson, R.; Evertsson, M. CFD simulation of a centrifugal air classifier used in the aggregate industry. *Miner. Eng.* **2014**, *63*, 149–156. [[CrossRef](#)]
20. Kapustin, F.L.; Perepelitsyn, V.A.; Ponomarev, V.B.; Loshkarev, A.B. Enhancing Efficiency of Rock Crushing Screening Utilization. *J. Min. Sci.* **2017**, *53*, 519–523. [[CrossRef](#)]
21. Petit, H.A.; Barbosa, M.R. Simulation of a cross-flow air classifier at high solid feed rates. *Rev. Int. Metodos Numer.* **2017**, *33*, 262–270.
22. Sakaguchi, E.; Suzuki, M.; Favier, J.F.; Kawakami, S. PH—Postharvest Technology: Numerical Simulation of the Shaking Separation of Paddy and Brown Rice using the Discrete Element Method. *J. Agric. Eng. Res.* **2001**, *79*, 307–315. [[CrossRef](#)]
23. Eswaraiah, C.; Kavitha, T.; Vidyasagar, S.; Narayanan, S.S. Classification of metals and plastics from printed circuit boards (PCB) using air classifier. *Chem. Eng. Process.* **2008**, *47*, 565–576. [[CrossRef](#)]
24. Ataş, S.; Tekir, U.; Paksoy, M.A.; Çelik, A.; Çam, M.; Sevgel, T. Numerical and experimental analysis of pulverized coal mill classifier performance in the Soma B Power Plant. *Fuel Process. Technol.* **2014**, *126*, 441–452. [[CrossRef](#)]
25. Johansson, R.; Evertsson, M. CFD simulation of a gravitational air classifier. *Miner. Eng.* **2012**, *33*, 20–26. [[CrossRef](#)]
26. Cao, M.; Yang, Y.; Wu, C.; Cai, C. A novel micro-spiral pneumatic selection system for the separation of fresh tea leaves. *Int. J. Food Eng.* **2021**, *17*, 595–608. [[CrossRef](#)]
27. Ciukaj, S.; Hernik, B. Field and CFD Study of Fuel Distribution in Pulverized Fuel (PF) Boilers. *J. Therm. Sci.* **2020**, *29*, 535–545. [[CrossRef](#)]
28. Yang, X. Kinematic Properties and Test of Plastics’ Optimal Separation Equipment. *J. Mech. Eng.* **2007**, *43*, 132–135. [[CrossRef](#)]
29. Johansson, R.; Evertsson, M. An empirical study of a gravitational air classifier. *Miner. Eng.* **2012**, *31*, 10–16. [[CrossRef](#)]
30. Zhang, R.; Yang, H.; Junfu, L.Ü. Application of CPFDF Approach on Gas-solid Flow and Combustion in Industrial CFB Boilers. *Proc. Chin. Soc. Electr. Eng.* **2013**, *33*, 75–83.
31. Sung, W.C.; Kim, J.Y.; Chung, S.W.; Lee, D.H. Effect of particle size distribution on hydrodynamics of pneumatic conveying system based on CPFDF simulation. *Adv. Powder Technol. Int. J. Soc. Powder Technol.* **2021**, *32*, 2336–2344. [[CrossRef](#)]